ADVANCES IN ATMOSPHERIC SCIENCES, VOL. 28, NO. 5, 2011, 1215–1232

Uncertainty of Climate Response to Natural and Anthropogenic Forcings Due to Different Land Use Scenarios

Alexey V. ELISEEV* and Igor I. MOKHOV

A. M. Obukhov Institute of Atmospheric Physics, Russian Academy of Sciences,

3 *Pyzhevsky,* 119017 *Moscow, Russia*

(Received 26 March 2010; revised 10 December 2010)

ABSTRACT

The A. M. Obukhov Institute of Atmospheric Physics, Russian Academy of Sciences (IAP RAS) climate model (CM) of intermediate complexity is extended by a spatially explicit terrestrial carbon cycle module. Numerical experiments with the IAP RAS CM are performed forced by the reconstructions of anthropogenic and natural forcings for the 16th to the 20th centuries and by combined SRES (Special Report on Emission Scenarios) A2–LUH (Land Use Harmonization) anthropogenic scenarios for the 21st century. Hereby, the impact of uncertainty in land–use scenarios on results of simulations with a coupled climate–carbon cycle model is tested. The simulations of the model realistically reproduced historical changes in carbon cycle characteristics. In the IAP RAS CM, climate warming reproduced in the 20th and 21st centuries enhanced terrestrial net primary production but terrestrial carbon uptake was suppressed due to an overcompensating increase in soil respiration. Around year 2100, the simulations the model forced by different land use scenarios diverged markedly, by about 70 Pg (C) in terms of biomass and soil carbon stock but they differed only by about 10 in terms of atmospheric carbon dioxide content.

Key words: terrestrial carbon cycle, climate model, anthropogenic scenarios, uncertainty in projections

Citation: Eliseev, A. V., and I. I. Mokhov, 2011: Uncertainty of climate response to natural and anthropogenic forcings due to different land use scenarios. *Adv. Atmos. Sci.*, **28**(5), 1215–1232, doi: 10.1007/s00376-010-0054-8.

1. Introduction

One of the largest achievements in climate modelling during the last decade has been the implementation of an interactive carbon cycle in three–dimensional climate models. This work was pioneered by Cox et al. (2000) and by Friedlingstein et al. (2001) and was followed by Brovkin et al. (2002, 2004), Matthews et al. (2004, 2005), Mokhov et al. (2006), Eliseev and Mokhov (2007), Eliseev et al. (2007a) and Volodin (2007). These studies showed that such interactive coupling enhances the build up of carbon dioxide (CO_2) in the atmosphere in comparison with a hypothetical case in which the carbon cycle is not affected by changes in climate. More recently, different climate models have been extended either by a partially interactive terrestrial methane cycle (e.g., Gedney et al., 2004; Eliseev et al., 2008; Volodin, 2008) or by interactions of carbon and nitrogen cycles (e.g., Thornton et al., 2007; Sokolov et al., 2008; Jain et al., 2009; Gerber et al., 2010; Zaehle et al., 2010b) with important implications for future changes in atmospheric CO_2 content q_{CO_2} (Eliseev, 2008; Thornton et al., 2007; Sokolov et al., 2008; Jain et al., 2009; Gerber et al., 2010; Zaehle et al., 2010b). Additional insights into carbon–cycle dynamics were obtained with respective box models (Svirezhev et al., 1999; Svirezhev and von Bloh, 1997, 1998; Eliseev and Mokhov, 2008; Mokhov and Eliseev, 2008; Ginzburg and Zavalishin, 2008). In particular, a globally averaged carbon–cycle module was implemented in a climate model (CM) of intermediate complexity developed at the A. M. Obukhov Institute of Atmospheric Physics, Russian Academy of Sciences (IAP RAS CM; Mokhov et al.,

*Corresponding author: Alexey V. ELISEEV, eliseev@ifaran.ru, eliseev_av@mail.ru.

2006; Eliseev and Mokhov, 2007; Eliseev et al., 2007a). While such globally averaged scheme allowed the projection of atmospheric content of CO_2, it lacked spatial resolution, and, as a result, did not allow the estimation of regional changes in carbon–cycle characteristics as well as interactive calculation of CO_2 emissions due to land-use activity; it was unable to properly couple the carbon cycle and other biogeochemical cycles, and it was limited in coupling between cycles of CO_2 and methane.

The goal of the present study is to describe simulations using the newly developed spatially explicit terrestrial carbon–cycle module that was implemented in the current version of the IAP RAS CM. The present version of the scheme allows the estimation of regional changes in terrestrial carbon stocks and fluxes as well as the simulation of direct CO_2 emissions due to land–use clearing. However, this version of the module neglects coupling the carbon cycle with other biogeochemical cycles. All of the papers mentioned above utilized SRES emission scenarios for future projections of carbon stocks and climate states. Recently, a new generation of land-use scenarios was developed under the framework of the Land Use Harmonization (LUH) project (Hurtt et al., 2009). Four LUH scenarios cover a wide range of possibilities for changes in extent of agricultural area. If an LUH scenario is combined with an SRES scenario for other anthropogenic forcings (i.e., fossil fuel and industrial CO_2 emissions and concentrations of other anthropogenic greenhouse gases and aerosols), the possible impact of uncertainty in land–use scenarios on simulation of climate and carbon cycle can be examined. Such a combination is a novel feature of simulations performed in this study. Simulations forced by different LUH scenarios diverged markedly in terms of terrestrial carbon stocks. However, for a given SRES scenario, they led to a rather narrow uncertainty range for atmospheric CO_2 concentration and, in turn, to a narrow uncertainty range for change in climate characteristics.

2. Model description

Previous versions of the IAP RAS CM (Petoukhov et al., 1998; Handorf et al., 1999; Mokhov et al., 2005; Eliseev et al., 2007b; Arzhanov et al., 2008; Eliseev et al., 2009) included a globally averaged carbon–cycle scheme described by Mokhov et al. (2006, 2008), Eliseev et al. (2007a), Eliseev and Mokhov (2007), Mokhov and Eliseev (2008). In the present study, a globally averaged terrestrial carbon–cycle scheme was replaced by a spatially explicit one. In the latter scheme, plant production and carbon stocks are updated annually to preserve the approximation of a well–mixed atmosphere with respect to CO_2. However, seasonally resolved time series of basic input variables for the preceding year are used as an input. These variables include surface air temperature $T_{\mathrm{a,s}}$, soil moisture fractional saturation w, and shortwave radiation balance at the surface R_{SW}. The latter variable is used as a proxy for the photosynthetically active radiation. The oceanic part of the IAP RAS CM carbon cycle is kept as a globally averaged module identical to the scheme FocNL described by Mokhov and Eliseev (2008), Mokhov et al. (2008). The latter is a Bacastow–type model (Bacastow, 1981) modified by taking into account temperature dependence of chemical reactions rates according to Millero (1995). The scheme is closed using the equation for the atmospheric CO_2 concentration in a well–mixed approximation

$$c_0 \frac{dq_{\mathrm{CO_2}}}{dt} = E_{\mathrm{ff}} + E_{\mathrm{lu}} + E_{\mathrm{fire}} - F_{\mathrm{l}} - F_{\mathrm{o}} \qquad (1)$$

where $q_{\mathrm{CO_2}}$ is atmospheric concentration of CO_2, t is time, c_0=2.123 Pg (C)/ppmv, E_{ff}, E_{lu}, and E_{fire} are global emissions of CO_2 due to fossil fuel burning+cement production, land–use clearing, and natural fires, respectively, and F_{l} and F_{o} represent global CO_2 uptakes by terrestrial ecosystems (land) and by the world ocean, respectively.

The new, spatially distributed terrestrial carbon–cycle module distinguishes six plant functional types (PFTs): tropical trees, temperate broadleaf trees, cool needleleaf trees, grasses, shrubs and crops. Grid cells in the model are divided in two parts covered by natural vegetation (one of the first five PFTs) and crops, respectively. Fractional areas occupied by these parts are denoted as a_{nat} and a_{agro}, respectively. Carbon masses per unit area in living vegetation and in soil were calculated using Eq. (A1) and Eq. (A11) shown in the Appendix. Two types of vegetation disturbance are considered: natural fires and land–use clearing. The latter type results in direct land–use CO_2 emissions that were calculated interactively by the model. Riverine carbon fluxes were neglected in the current version of the model. Explicit interaction of carbon cycle with other biogeochemical cycles was neglected in the current version of the scheme as well. A detailed description of the terrestrial carbon–cycle module is given in the Appendix.

3. Numerical experiments

Numerical experiments with this version of the IAP RAS CM were performed for the period 1500–2100. For the 16th–20th centuries, these simulations

were forced using the reconstructed annual fossil fuel emissions (Marland et al., 2005), atmospheric concentrations of nitrous oxide and methane (MacFarling Meure et al., 2006, freons CFC–11 and CFC–12 (Walker et al., 2000), tropospheric burdens of sulphate aerosols (Horowitz, 2006), annual mean solar irradiance (Wang et al., 2005), and seasonally averaged stratospheric aerosol optical depth [annual mean data (Robertson et al., 2001) until year 1889 and monthly mean arrays (Ammann et al., 2003) thereafter]. The fraction of the model grid cell covered by permanent agriculture a_{agro} is obtained from the Land Use Harmonization project home site (http://luh.unh.edu/data.shtml) and was based on the History Database of the Global Environment (HYDE), version 3.1 dataset (Klein Goldewijk, 2001). Crop/pasture area, a_{agro} was used to force both the carbon cycle and the surface albedo routines of our model. In the 21st century, fossil fuel CO_2 emissions and atmospheric concentrations of N_2O, CH_4, CFC–11 and CFC–12 were prescribed in accordance with the SRES A2 scenario (Houghton et al., 2001). The total column burden of tropospheric sulphates was adopted from the corresponding simulation performed with the MOZART (Model for OZ one and Related chemical Tracers), version 2 chemical–transport model (Horowitz, 2006). The 21st–century land–use scenarios were chosen based on the simulations with the integrated assessment models AIM (Asian Pacific Integrated Model), IMAGE (Integrated Model to Assess the Global Environment), MESSAGE (Model for Energy Supply Strategy Alternatives and their General Environmental Impact), and MiniCAM (Mini–Climate Assessment Model) as performed in the framework of the LUH project. For all such models, version 1 of the data was used, except the IMAGE model for which the version 1.1_rc1 was employed). Possible volcanic eruptions and solar irradiance variations were not considered for the 21st century.

LUH scenarios were developed using the four models listed in the previous paragraph. These projections differed from each other despite the identical protocol of performed simulations. Among these scenarios, the most aggressive was calculated using the MESSAGE model. In this scenario, a_{agro} increased (relative to the value for year 2000) monotonically in the 21st century, by 8% in 2050, and by 13% in 2100. This increase occurred worldwide. A similar but smaller increase of a_{agro} was simulated using the IMAGE model. In the latter scenario, area of crops and pastures increased by 3% from year 2000 to year 2080, with a very slight decrease thereafter. The most heterogeneous changes of a_{agro} were simulated using the AIM model. In this projection, total a_{agro} increased by 6% between 2000 and 2060. In this model the extent of a_{agro} increased in most regions of the world. However, localized decreases of a_{agro} were simulated in central Europe, south of the Caspian Sea, and in the southern parts of Africa and South America. During 2060–2100, the AIM model projected the return of the global extent of a_{agro} to the value characteristic for the year 2000. In turn, in the MiniCAM projection, global extent of a_{agro} decreased by 19% during the 21st century. This decrease occurred worldwide but with minor increases in China, in the northern subtropics of Africa, and in the northernmost regions of Eurasia and North America.

All of the simulations presented in this paper were initialized from the model's equilibrated preanthropogenic state with $a_{\text{agro}} \equiv 0$ and $E_{\text{ff}} \equiv 0$. At astronomical year 1500, a_{agro} was replaced by the respective fields adapted from the LUH database. The latter allowed the consideration of direct land–use clearing emissions not only for the nominal period of simulation but for the whole anthropogenic period. The LUH fields also provided that natural vegetation carbon stock per unit area in undisturbed areas changed little (e.g., due to climate changes or due to plant fertilization by atmospheric CO_2) during the early stage of anthropogenic period.

4. Results

Temperature, precipitation, and soil moisture fields simulated by the IAP RAS CM under SRES scenarios have been analyzed previously (e.g., Eliseev et al., 2009; Eliseev and Mokhov, 2011). Therefore, their detailed analyses have been omitted from the present paper. In brief, our model reproduced the temperature increase of 0.7°C during the 20th century (which agrees with observation data (Solomon et al., 2007), and the spatial pattern of surface air temperature change in our model is realistic. Precipitation increase was slightly overestimated during the 20th century in comparison to observation data (Solomon et al., 2007). Under the SRES A2 scenario, the model projected temperature increased by 2.7°C during the 21st century. This number agrees with the lower range of the IPCC AR4 simulations (Solomon et al., 2007). This result is consistent with the relatively small equilibrium sensitivity of our model to the doubling of the CO_2 content in the atmosphere which equals 2.2°C. The major drawback of the IAP RAS CM is its high positive precipitation sensitivity to temperature increase, which is larger than that of other contemporary climate models (e.g., Petoukhov et al., 2005). The possible impact of the latter drawback on the results obtained in this study is discussed in section 5.2.

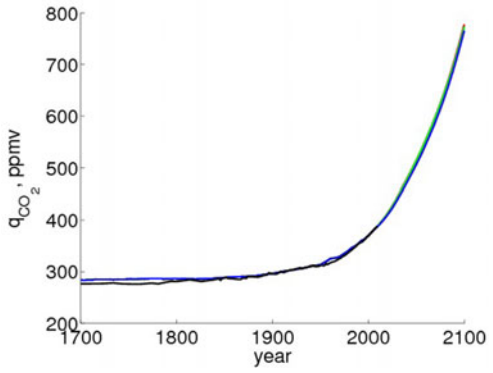

Fig. 1. Global atmospheric concentration of CO_2 simulated by the IAP RAS CM under scenarios AIM, IMAGE, MESSAGE, and MiniCAM (green, magenta, red, and blue curves correspondingly) for changes in area of crops/pastures and under scenario SRES A2 for other anthropogenic forcings. Black line depicts the respective Law Dome borehole data (MacFarling Meure et al., 2006) prior to 1958 and Mauna Loa measurements (Keeling et al., 1996) thereafter.

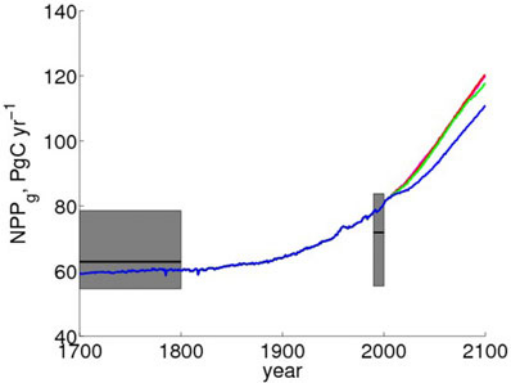

Fig. 2. Global modelled net primary production (color lines). Gray boxes depict respective ranges obtained for the C^4MIP ensemble by (Arora and Matthews, 2009) with ensemble mean value shown by black line. Curve notations are the same as used in Fig. 1.

4.1 *Preindustrial state*

During the preanthropogenic spin–up phase, no statistically significant trends were found for any model variable, either at the global scale or in any model grid cell. In the year 1500, coupling shock resulted in pulse emission of 19 Pg (C) in the atmosphere. The excess of CO_2 was taken up by the ocean (primarily) and by terrestrial biosphere within 30 years. From the mid–16th century until the late 18th century, the trends were small in comparison to those that developed in the 20th and 21st centuries.

In the early anthropogenic period (16th–18th centuries) globally averaged surface air temperature was 13.6°C±0.1°C (mean±interannual standard deviation) and globally averaged annual precipitation amounted 90.5±0.5 cm yr^{-1}. Atmospheric CO_2 concentration in this period was 283.7±1.7 ppmv (Fig. 1), in agreement with the Law Dome borehole data (MacFarling Meure et al., 2006).

Global terrestrial gross primary production was 116.6±0.8 Pg (C) yr^{-1}. This value is in general agreement with satellite–retrieved estimates for 2001–2003, 102–126 Pg (C) yr^{-1} (Zhao et al., 2006). Global net primary production (NPP) NPP_g was 59.4±0.6 Pg (C) yr^{-1} (Fig. 2). This agrees with a satellite–retrieved range, 47–74 Pg (C) yr^{-1} (Zhao et al., 2006) and with a range obtained in simulations with terrestrial carbon cycle models, 44–79 Pg (C) yr^{-1} (Cramer et al., 1999; Golubyatnikov and Denisenko, 2001; Arora and Matthews, 2009). Net primary production f_{NPP} per unit area was above 1 kg (C) m^{-2} in the tropical forests, in south–eastern Asia and in the Near East/Caucasian region (Fig. 3a). In steppes and temperate forests, f_{NPP} was 0.3–0.6 kg (C) m^{-2}. In the boreal regions, it was 0.1–0.3 kg (C) m^{-2}, and in tundra it was < 0.1 kg (C) m^{-2}. These values are in general agreement with empirical upscale estimations by (Luyssaert et al., 2007; Houlton et al., 2008). In addition, they agree with values obtained for the ensemble of the terrestrial carbon cycle models (Cramer et al., 1999) shown in Fig. 3b. Exceptions from the latter were overestimated f_{NPP} in the south–eastern part of Europe and in eastern Asia and overestimated f_{NPP} in the tropics and subtropics of the South America. However, different models simulated very diverse values of f_{NPP} in these regions (Cramer et al., 1999) leading to intermodel range which embeds values simulated by our model.

The IAP RAS CM–simulated carbon flux from natural fires was about 0.25 Pg (C) yr^{-1} at a global scale. This is smaller than estimates by Schultz et al. (2008). However, the latter estimate includes both natural and anthropogenic fires and suffers from large uncertainty. Modelled fire emissions of CO_2 reached $(2–5)\times10^{-3}$ kg (C) m^{-2} yr^{-1} in forested tropical and subtropical regions and diminished to the values $< 1 \times 10^{-3}$ kg (C) m^{-2} yr^{-1} in extratropical regions.

Global vegetation carbon stock during the indicated period was $C_{\mathrm{v}} = 623 \pm 5$ Pg (C) (Fig. 4). These values for C_{v} are within the ranges for empirical estimates, 466–654 Pg (C) (Houghton et al., 2001), as well as for simulations by by other state-of-the-art terrestrial carbon cycle models, 500–950 Pg (C) (Cramer et al., 2001). Preindustrial vegetation carbon stock per unit area c_{v} was < 2 kg (C) m^{-2} in subpolar latitudes (Fig. 5a). It increased in the subtropics up to 8–10 kg (C) m^{-2}, and reached 10–12 kg (C) m^{-2} in

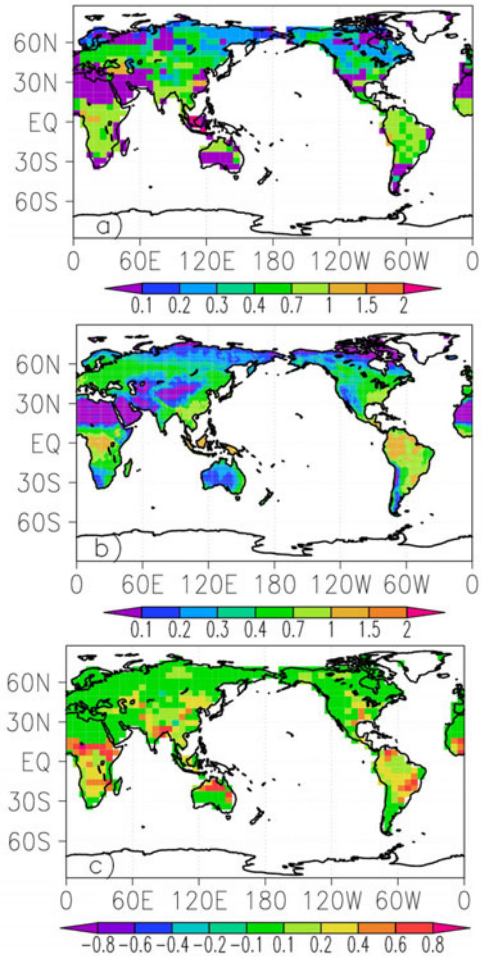

Fig. 3. Net primary production f_{NPP} simulated by the IAP RAS CM [kg (C) m^{-2} yr^{-1}] for years 1550–1700 (a) in comparison to that simulated by global models of terrestrial net primary productivity (Cramer et al., 1999) (b) and f_{NPP} change from 1550–1700 to 1995–2005 (c).

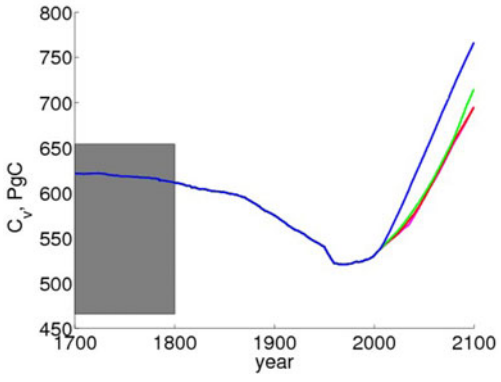

Fig. 4. Global modelled vegetation carbon stock (colour lines) in comparison to the data synthesis (Houghton et al., 2001) (gray box). Curve notations are the same as used in Fig. 1.

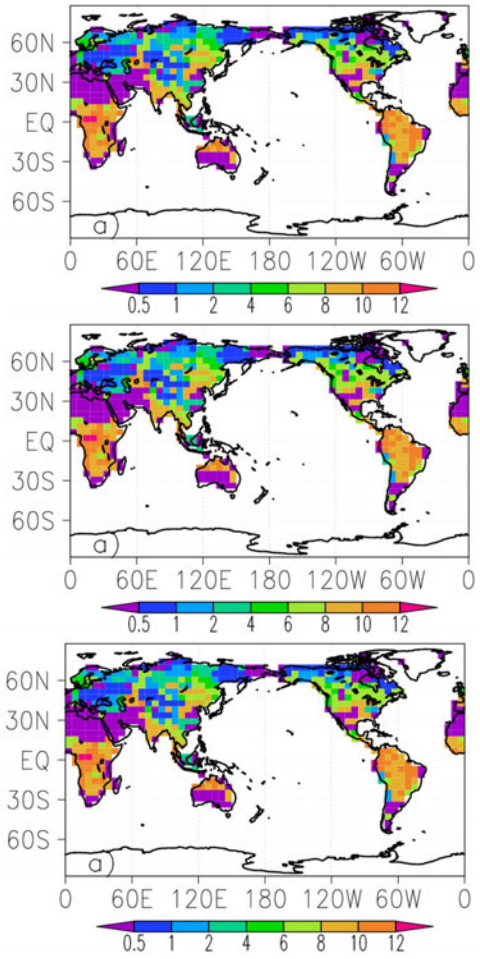

Fig. 5. Vegetation carbon stock c_{v} simulated by the IAP RAS CM [kg (C) m^{-2}] for years 1550–1700 (a), the respective data (Olson et al., 1985) (b), and c_{v} change from 1550–1700 to 1995–2005 (c).

the tropical forest area. These values are in general agreement with the gridded data by Olson et al. (1985) (Fig. 5b) and with the ecosystem–level data synthesis (Houlton et al., 2008; Luyssaert et al., 2007). The exceptions are the steppe regions where c_{v} was underestimated in comparison to (Houlton et al., 2008; Olson et al., 1985) and off–equatorial regions covered by tropical forest where carbon in living biomass was higher than reported by Olson et al. (1985).

Global preindustrial soil carbon stock was $C_{\mathrm{s}} = 1849 \pm 6$ Pg (C) (Fig. 6). The value for C_{s} agreed with empirical estimates 1993 ± 480 Pg (C) (Jobbágy and Jackson, 2000) and 2179 Pg (C) (Hall et al., 2005). Spatially, soil carbon stock per unit area c_{s} was extremely small in desert regions, it was 5–10 kg (C) m^{-2} in the tropics, was 20–30 kg (C) m^{-2} in regions covered by grasslands and temperate forests, and was > 30 kg (C) m^{-2} in subpolar regions (Fig. 7a). This values generally agree with the data (Hall et al., 2005)

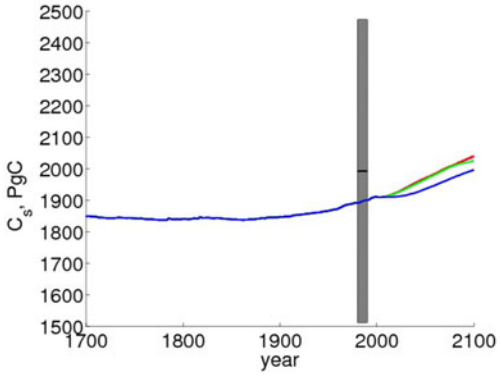

Fig. 6. Global modelled soil carbon stock (colour lines) in comparison to the data (Jobbágy and Jackson, 2000) (black line for central estimate and gray box for uncertainty range). Curve notations are the same as used in Fig. 1.

with an exception of underestimated c_s in deserts and overestimated c_s in the midlatitudinal steppes and temperate forests. However, for the latter case, the data–set (Hall et al., 2005) was for the upper 1.5 m of the soil column and did not consider deeper soil layers. These deeper layers in the indicated regions may bear as much as 30%–50% of organic soil carbon (Jobbágy and Jackson, 2000), and, consequently, total soil carbon stock may be markedly larger than figured by Hall et al. (2005). Further, the IAP RAS CM–simulated values of c_s were in general agreement with the ecosystem–level data synthesis (Houlton et al., 2008), including steppes and temperate forests.

4.2 *Changes during the historical period*

4.2.1 *Carbon fluxes*

During the 17th–20th centuries NPP_g increased by about 1/3 (Fig. 2). This increase is in general agreement with estimates by (Arora and Matthews, 2009. The NPP_g growth during the last two decades of the 20th century, from 76–77 Pg (C) yr^{-1} to about 81 Pg (C) yr^{-1}, agrees favorably with the estimate by Nemani et al. (2003) who showed that NPP has increased by 6% during a similar period. This change is basically due to the CO_2 fertilization effect. The dominant impact of plant fertilization by CO_2 is also visible in geographical distributions of f_{NPP} change during the historical period with the largest increases exhibited in the regions with large preindustrial NPP (Fig. 3c). After volcanic eruptions, terrestrial NPP_g was slightly reduced due to overall cooling. At a global scale, this result agrees with the tree–ring data analysis by Krakauer and Randerson (2003) but contrasts with the measurements in the northern hardwood forest performed by Gu et al. (2003). However, in some

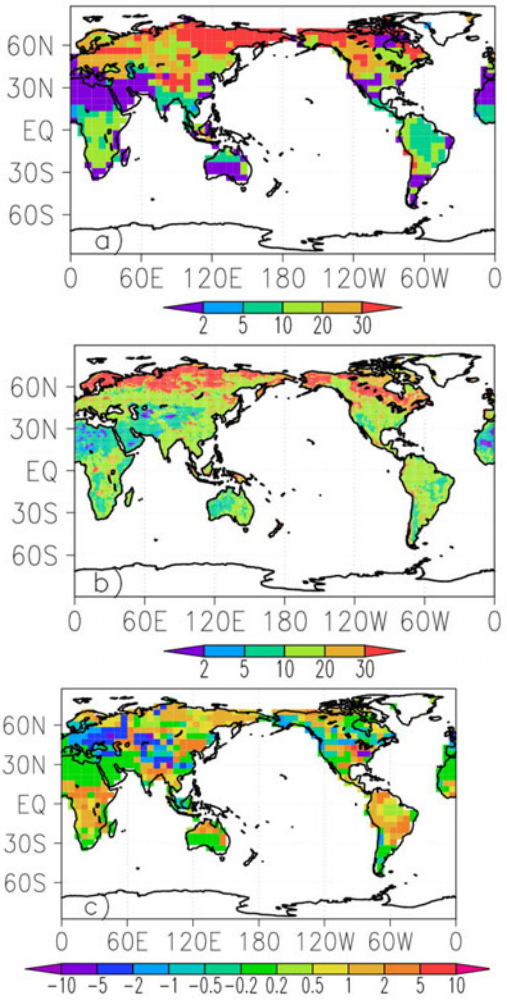

Fig. 7. Soil carbon stock c_s simulated by the IAP RAS CM [kg (C) m^{-2}] for years 1550–1700 (a) the corresponding data (Hall et al., 2005) (b), and c_v change from 1550–1700 to 1995–2005 (c).

regions covered by such forests, the model exhibits increased f_{NPP} after volcanic eruptions similar to Gu et al. (2003) due to development of climate conditions more favorable for vegetation.

Global modeled cumulative carbon emissions due to land–use clearing were 55 Pgc in 1500–1850 and were 155 Pg (C) in 1850–2000. The first number is within the range of other estimates, 48–79 Pg (C) (DeFries et al., 1999; Olofsson and Hickler, 2008; Pongratz et al., 2009). The total modeled land-use CO_2 emissions till year 2000, 210 Pg (C), are slightly above those obtained by DeFries et al. (1999); Olofsson and Hickler (2008) and Strassmann et al. (2008) but they are markedly smaller than those figured by Pongratz et al. (2009).

CO_2 emissions due to natural fires increased during the historical period and reached 0.30 Pg (C) yr^{-1}

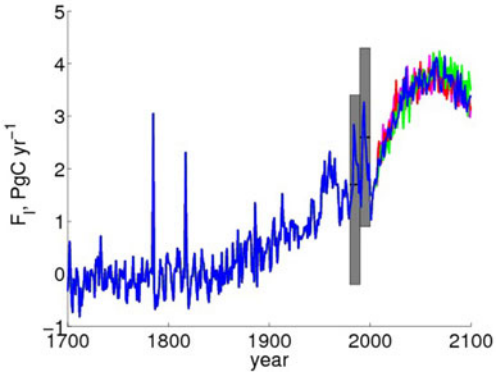

Fig. 8. Global modelled terrestrial carbon uptake (colour lines) in comparison to the observational estimations (Solomon et al., 2007) (black lines show central values and grey boxes depict uncertainty ranges). Curve notations are the same as used in Fig. 1.

in the late 20th century. This increase was due to juxtaposed CO_2 fertilization effect (leading to larger fuel stock) and climate effects composed from an extended growing period and from gradual depletion of soil moisture (both promote longer fire season and more frequent fires).

Global terrestrial carbon uptake F_l gradually increased from the 17th to the 20th centuries (Fig. 8). This increase was 1.9 Pg (C) yr^{-1} in 1980s and 2.2 Pg (C) yr^{-1} in 1990s. These values are within the respective observational uncertainty ranges from -0.2 Pg (C) yr^{-1} to 3.4 Pg (C) yr^{-1} with the central estimate of 1.7 Pg (C) yr^{-1} and from 0.9 Pg (C) yr^{-1} to 4.3 Pg (C) yr^{-1} with the central estimate 2.6 Pg (C) yr^{-1} (Solomon et al., 2007). Cumulative terrestrial carbon uptake during 1800–1994 in the model was 134 Pg (C) and agreed with the corresponding empirical estimates 61–141 Pg (C); cumulative terrestrial carbon uptake in the model during 1980–1999 was 43 Pg (C) and agreed with the corresponding empirical estimates 39 ± 18 Pg (C) (Sabine et al., 2004). The modeled value for 1800–1994 was in the upper range of the empirically estimated range. The latter, at least partly, was due to difference in definitions of land–use emissions: while our model estimated only direct emissions and places other emissions in carbon–cycle dynamics (see Appendix), the conventional bookkeeping estimates [which consider both direct and indirect land-use emissions (see Houghton et al., 1983)] were employed by Sabine et al. (2004).

Negative excursions of F_l are visible after major volcanic eruptions. This occurred despite the diminished f_{NPP} for these years and basically due to cooling–suppressed heterotrophic respiration. Similar reduction of soil respiration based on observations was previously noted by Jones and Cox (2001).

Terrestrial carbon uptake per unit area f_l was positive almost everywhere during the 17th to 20th centuries. In the late 20th century, its typical values ranged from 0.02 kg (C) m^{-2} yr^{-1} to 0.1 kg (C) m^{-2} yr^{-1} in tropical forests and from 0.01 kg (C) m^{-2} yr^{-1} to 0.05 kg (C) m^{-2} yr^{-1} in middle and subpolar latitudes.

Global oceanic carbon uptake also increased during the historical period (not shown). Its values averaged for 1980–1989, 1990–1999, and 2000–2005 equal to 1.6 Pg (C) yr^{-1}, 1.9 Pg (C) yr^{-1}, and 2.1 Pg (C) yr^{-1}, respectively, and fall in the corresponding empirical uncertainty ranges 1.8 ± 0.8 Pg (C) yr^{-1}, 2.2 ± 0.4 Pg (C) yr^{-1}, and 2.2 ± 0.5 Pg (C) yr^{-1} (Solomon et al., 2007). Cumulative oceanic carbon uptake during 1800–1994 in the model was 114 Pg (C) and during 1980–1999 it was 37 Pg (C). These values are in excellent agreement with the respective empirical estimates of 118 ± 19 Pg (C) for 1800–1994 and 37 ± 8 Pg (C) for 1980–1999 (Sabine et al., 2004).

4.2.2 *Carbon stocks*

Despite enhanced NPP, vegetation carbon stock decreased by about 1/4 until the mid–20th century (Fig. 4). This decrease occurred due to replacement of natural vegetation by crops and pastures with a faster carbon turnaround (Table A3). Spatially, changes of c_v reflected mutual compensation of NPP increase and faster carbon loss from vegetation to soil due to land–use clearing (Fig. 5c). The former effect dominated in the agriculture–free regions while the latter one was visible in the subtropics and middle latitudes where land use was more intensive during the 17th–20th centuries. In tropical forests, the simulated carbon stock increased during the last two decades of the 20th century varied from 0.01 kg (C) yr^{-1} to 0.02 kg (C) yr^{-1} which was slightly below the field estimate of 0.03–0.07 kg (C) m^{-2} yr^{-1} (Lewis et al., 2009).

Total soil carbon stock slightly decreased until the late 19th century and then increased until year 2000 by $\sim$ 70 Pg (C) (Fig. 6). This increase was a result of losses of soil carbon in agricultural regions and respective gains in agriculture–free areas (Fig. 7c).

Carbon dioxide atmospheric content was stable until early 19th century. Then it started to increase, and it reached 370 ppmv in year 2000 (Fig. 1). This value is in excellent agreement with the Mauna Loa observations (Keeling et al., 1996 and update).

4.3 *Projections for the* 21st *century*

4.3.1 *Carbon fluxes*

In the 21st century, NPP_g increased to 110–120 Pg (C) yr^{-1} depending on the chosen land–use scenario (Fig. 2). This increase was larger for scenarios imply-

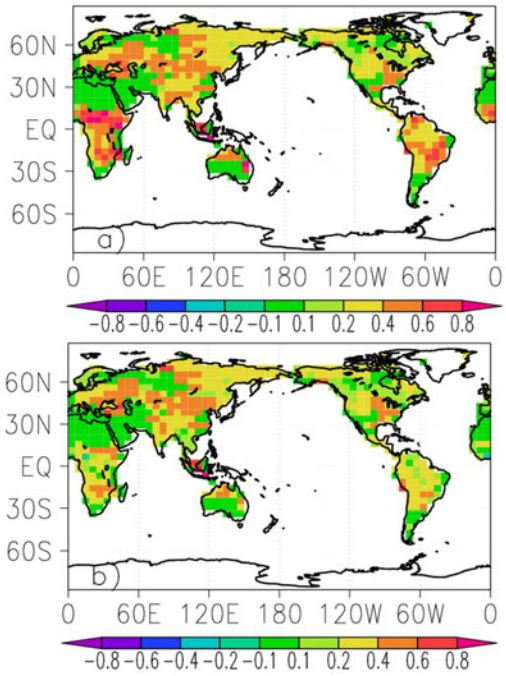

Fig. 9. Net primary production change [kg (C) m^{-2} yr^{-1}] from 1995–2005 to 2090–2100 simulated under scenarios MESSAGE (a) and MiniCAM (b) for area of crops/pastures and scenario SRES A2 for other anthropogenic forcings.

ing further land–use clearing in the 21st century (IMAGE and MESSAGE) and was smaller for the MiniCAM scenario in which agricultural area decreased during this period. Terrestrial NPP simulated for the late 21st century was above the range exhibited in Coupled Climate–Carbon Cycle Project (C^4MIP) which is from 90 Pg (C) yr^{-1} to 110 Pg (C) yr^{-1}.ne model participated in this project simulated NPP_g at $\sim$ 130 Pg (C) yr^{-1} around year 2100). The reason for this difference was due to the set up of the simulations used in the present study that were not identical to the set up of the C^4MIP runs. In particular, in the latter intercomparison, land–use emissions were prescribed according to the precomputed SRES A2 scenario (Houghton et al., 2001) rather than diagnosed from the model. In additional simulations with the model arranged in a way similar to that used in the C^4MIP, global terrestrial NPP in the late 21th century was 93 Pg (C) yr^{-1}, which was close to the middle of the range calculated in the C^4MIP runs. Comparison of these results with the results of simulations where individual processes contributing to carbon–cycle dynamics were suppressed artificially suggests that plant fertilization by atmospheric CO_2 was yet significant in the 21st century, and that climate changes further enhance terrestrial NPP. The latter contrasts with most of the C^4MIP models in which climate change suppresses NPP, while some of them do show NPP_g enhancement from uncoupled run to the coupled simulation. Climate–induced NPP increase was also exhibited in the experiments with the ISAM model (Jain et al., 2009).

Our model projects enhanced NPP in most regions during the 21st century except in deserts (Figs. 9a, b). The typical values of f_{NPP} increases range from 0.2 kg (C) m^{-2} yr^{-1} to 0.6 kg (C) m^{-2} yr^{-1} in the extratropics. In tropical forests, where the largest divergence between different land–use scenarios was found, increases of f_{NPP} were the most marked [from 0.4 kg (C) m^{-2} yr^{-1} to 0.8 kg (C) m^{-2} yr^{-1} in central Africa and from 0.2 kg (C) m^{-2} yr^{-1} to 0.6 kg (C) m^{-2} yr^{-1} in South America] for scenarios implying further land–use clearing (Fig. 9a), and they were smaller [from 0.2 kg (C) m^{-2} yr^{-1} to 0.4 kg (C) m^{-2} yr^{-1}] for the MiniCAM scenario (Fig. 9b).

Reflecting imposed scenarios of clearing, land–use emissions were close to zero for the MiniCAM scenario. These values for the other three land–use scenarios were not zero but they basically diminished during the 21st century approaching 0.1 Pg (C) yr^{-1}–0.4 Pg (C) yr^{-1} in its last decades. Cumulative carbon emissions due to land–use clearing for the whole 21st century range from 4 Pg (C) for the MiniCAM scenario to 46 Pg (C) for the MESSAGE scenario.

CO_2 emissions due to natural fires continued to increase during the 21st century. In the last decades of this century, these emissions attained 0.4 Pg (C) yr^{-1}. Spatially, they were most important in tropical and temperate forests, with their high biomass and warm temperatures. However, as shown by additional simulations where natural fires CO_2 emissions were either suppressed or enhanced artificially, the impact of natural fires on global carbon budget in the model was fairly small.

Global terrestrial carbon uptake increased until the 2060s, when it reached 3.8–3.9 Pg (C) yr^{-1} (Fig. 8). Afterward, carbon uptake declined approaching 3.4–3.5 Pg (C) yr^{-1} in the late 21st century. Spatially, terrestrial carbon uptake did not change drastically among different land–use scenarios in the 21st century. This was due to the relatively small changes in the extent of crops and pastures among different LUH scenarios. Terrestrial carbon uptake per unit area f_l is positive in most vegetation–covered regions, especially in tropical forests, where it was consistently > 0.05 kg (C) m^{-2} yr^{-1} in the last 10 years of the 21st century (Fig. 10). However, regions of negative f_l were exhibited in agricultural regions of southern Russia, in northern North America and in western Africa. In all of these regions, $f_l < 0$ was caused by the enhanced heterotrophic respiration r_s overcoming the NPP in-

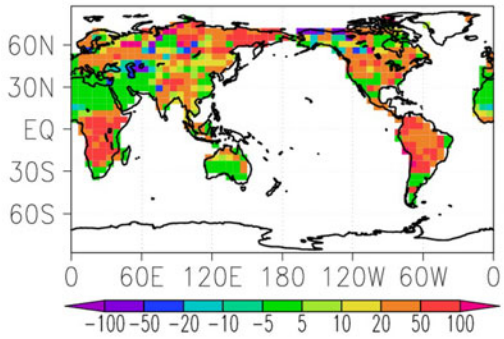

Fig. 10. Terrestrial carbon uptake [$10^{-3}\times$ kg (C) m^{-2} yr^{-1}] in 2090–2100 simulated simulated under scenarios MESSAGE for area of crops/pastures and scenario SRES A2 for other anthropogenic forcings.

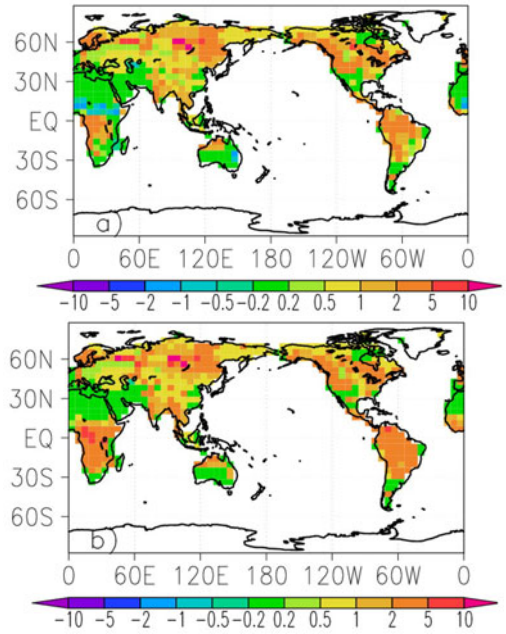

Fig. 11. Change in vegetation carbon stock [kg (C) m^{-2}] from 1995–2005 to 2090–2100 simulated simulated under scenarios MESSAGE (a) and MiniCAM (b) for area of crops/pastures and scenario SRES A2 for other anthropogenic forcings.

crease. In the first region, the latter enhancement was due to continuing agricultural activity. In contrast, in the latter two regions, it was induced by climate changes, in particular by increased fire activity.

Oceanic uptake of CO_2 continued to increase during the 21st century. In the last 10 years of this century, it reached 9.7–9.9 Pg (C) yr^{-1}.

4.3.2 *Carbon stocks*

Vegetation carbon stock increased to $\sim$ 700 Pg (C) during the 21st century. This increase was basically due to plant fertilization by atmospheric CO_2 and was the largest for the MiniCAM scenario.

Spatial changes in vegetation carbon stock basically followed those for NPP. For instance, strong NPP increase [by 2–10 kg (C) m^{-2}] was projected over the extratropical land in the 21st century (Fig. 11a, b). In the tropics and subtropics, the simulations performed under different land–use scenarios diverged more markedly due to land–use clearing (if the latter occurred in the given scenario) compensating increases of NPP. In particular, vegetation carbon increased for the MiniCAM scenario (Fig. 11b) by 2–10 kg (C) m^{-2}. For scenarios with further land–use clearing, c_v growth in the tropics was smaller, typically by 2–5 kg (C) m^{-2}, and a vegetation decrease of 0.5–2 kg (C) m^{-2} was projected in the northern part of the African region covered by tropical forests (Fig. 11a).

Global soil–carbon stock increased to 1994–2038 Pg (C) during the 21st century (Fig. 4). Soil carbon stock per unit area basically increased in the tropics by 1–5 kg (C) m^{-2} (Fig. 12). In the extratropics, c_s inreased in grasslands, temperate forests, and in tundra by 1–5 kg (C) m^{-2} but decreased in boreal regions by 1–10 kg (C) m^{-2}.

Atmospheric CO_2 concentration in the 21st century grew up to 752–763 ppmv under the SRES A2 emission scenario depending on the imposed land–use scenario (Fig. 1). These values were at the lower end of the range 730–1020 ppmv exhibited in the C^4MIP simulations. In our model, about 90 ppmv of this growth was due to interactions between climate and carbon cycle as shown in additional simulations in which climate-carbon cycle coupling was suppressed artificially. In turn, the most part of this additional growth, about 85 ppmv was due to the impact of climate changes on the terrestrial carbon cycle.

While different land–use scenarios employed here

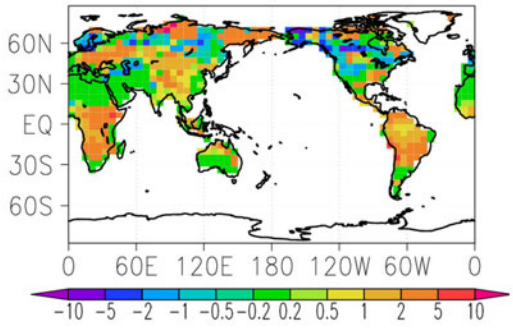

Fig. 12. Change in soil carbon stock from 1995–2000 to 2090–2100 [kg (C) m^{-2}] simulated simulated under scenarios MESSAGE for area of crops/pastures and scenario SRES A2 for other anthropogenic forcings.

diverged markedly, by $\sim$ 70 Pg (C), in terms of biomass and soil carbon stock, they differed only by $\sim$ 10 ppmv in terms of atmospheric CO_2 content.

5. Conclusions

5.1 *Summary of the results*

In this paper, a description of the new terrestrial carbon cycle module adopted to suit a climate model of intermediate complexity has been presented. The module was implemented in the model developed at the IAP RAS CM. With the coupled model, simulations were performed for the 16th to the 21st centuries. The forcings in these simulation were based on the respective reconstructions for the 16th to the 20th centuries. For the 21st century, anthropogenic forcings were prescribed according to the SRES A2 scenario (except the extent of crops/pastures, which was adapted from the LUH project scenarios), and possible natural forcings were neglected.

The model simulations were in general agreement with empirical estimates of terrestrial plant production and carbon stocks in vegetation and soil for the 19th to the 20th centuries. The model realistically reproduced measured historical changes of carbon-cycle characteristics such as decadal- and centennial-scale enrichment of the Earth's atmosphere by CO_2, terrestrial and oceanic carbon uptakes, and direct land–use CO_2 emissions. For all of these variables, the results of the simulations presented here were comparable either with empirical data or (if such data were unavailable) with calculations performed using other state-of-the-art climate-carbon cycle models. While some differences from the C^4MIP output were noted for the IAP RAS CM, they can be traced to the differences in the experimental protocols between the present study and the C^4MIP runs.

In our model, climate warming reproduced in the 20th and 21st centuries enhanced terrestrial NPP. This feature is not in accordance with the major part of the C^4MIP ensemble, but it agrees with some models participating in this project and with the ISAM model, which was not included in the latter intercomparison but was used extensively in the Intergovernmental Panel on Climate Change Assessment Reports (Houghton et al., 2001; Solomon et al., 2007). In the 21st century, the IAP RAS CM projections showed continuing growth of CO_2 up to 752–763 ppmv under the SRES A2 emission scenario, depending on the imposed land–use scenario. This result was accompanied by increased carbon stocks in vegetation and soil, by 68–137 Pg (C) (160–230 Pg (C)) and by 145–189 Pg (C) (54–128 Pg (C)), correspondingly, relative to the model's preanthropogenic state (late 20th century). Despite the climate-enhanced NPP, global warming in the model suppressed terrestrial and oceanic carbon uptakes because heterotrophic respiration overcompensated this NPP increase, imposing an overall positive climate–carbon cycle feedback. The latter occurred despite the fact that soil carbon stock was increased rather than depleted in the 21st century. Similar behavior is characteristic for the IPSL–CM2 general circulation model [Fig. 3 in Friedlingstein et al. (2006)].

A novel feature of the simulations performed here is that they combined LUH project scenarios for the extent of crops and pastures with the conventional SRES A2 scenario for fossil fuel+industrial CO_2 emissions and concentrations of other anthropogenic greenhouse gases and tropospheric sulphates. Overall, different land–use scenarios employed here diverged markedly, by $\sim$ 70 Pg (C), in terms of biomass and soil carbon stock, but they differed only by $\sim$ 10 ppmv in terms of atmospheric CO_2 content.

In all simulations included the present study, both terrestrial NPP_g and soil respiration increased in a warmer climate and decreased in a colder one. However, the latter variable appeared to be more sensitive with respect to temperature changes than the former one. This effect led to a positive climate–carbon cycle feedback in our model as well as in other state–of–the–art climate models with an interactive carbon cycle (Friedlingstein et al., 2006). This positive feedback in our model was exhibited for both century–scale climate changes and for climate variations occurring after volcanic eruptions. However, current understanding of the climate–carbon cycle interaction was unable to constrain this feedback. This was reflected, for instance, in the wide range of climate–carbon cycle feedback intensity simulated in the C^4MIP intercomparison. Moreover the work of Jones et al. (2006), Eliseev and Mokhov (2007), and Eliseev (2008) showed that even negative climate–carbon cycle feedback is consistent with the currently available observational data.

While this topic is beyond the scope of the present study, we note, in this respect, an additional ensemble simulation performed with the IAP RAS CM in Eliseev (2011). In the latter simulation, individual ensemble members were constructed by sampling two global parameters conditioning the dynamics of terrestrial carbon cycle. Despite wide ranges of values for both parameters employed in Eliseev (2011), on a global basis, NPP enhancement occurred in all ensemble members for both in long–term and interannual post–volcanic climate changes. Moreover, an increase of F_l after volcanic eruptions was also robust within this ensemble. In the future, we plan to perform additional simulations by sampling other model parameters to further

test NPP and F_l sensitivities to climate changes.

5.2 *Caveats*

Notably, the current version our model is not free from caveats. Among these is a neglect of interactions between the carbon cycle and other biogeochemical cycles. In particular, interactions of the carbon cycle with the nitrogen cycle could modify substantially the response of carbon cycle to external forcing (e.g., Sokolov et al., 2008; Zaehle et al., 2010a). Moreover, nitrogen–cycle functioning currently is strongly modified by human activities such as the use of fertilizers in agricultural practice. In particular, different scenarios of fertilizer usage may lead to different responses of the carbon–cycle system to the same scenario for changes in area covered by crops and/or pastures. This opens a possible direction of research to study impact of agricultural area spread on uncertainty of projected climate and carbon–cycle characteristics.

As stated in the Introduction, our model is characterized by high precipitation sensitivity to climate warming. This may affect carbon fluxes between atmosphere and terrestrial reservoirs. While it is difficult to assess this impact directly, additional simulations were performed with only the preindustrial climatology for soil moisture content entering terrestrial carbon cycle module. In this extreme case of zero precipitation sensitivity to external forcing, NPP and change of carbon stock in vegetation was very similar to that obtained with the standard version of the model. However, accumulation of carbon in soil during the 21st century was enhanced by ~ 60 Pg (C) in this additional simulation with respect to that obtained in simulations with the standard version of the model. In turn, a corresponding q_{CO_2} increase was suppressed by ~ 30 ppmv. Taking into account that this assessment of precipitation sensitivity is an extremal one, we conclude that its impact is rather small in comparison to changes simulated by the model during the 21st century (see section 4.3.2). Moreover, the main conclusion of the present study, the small impact of difference between LUH scenarios on spread of projected CO_2, remains unaffected.

In addition, the simplified, globally averaged scheme for oceanic carbon uptake in the model may overlook the possible impact of changes in oceanic circulation on oceanic carbon uptake (Friedlingstein et al., 2006). However, according to the results reported by Zickfeld et al. (2008), this effect was quite modest in the 21st century. Furthermore, the likely impact of oceanic changes on the carbon cycle is to shift the q_{CO_2} trajectory averaged over different land–use scenarios rather than to change a spread between them provided that the latter is narrow enough.

5.3 *Tentative implication for geoengineering climate mitigation*

The results obtained in the present study may have some implications for the climate geoengineering by stratospheric sulphates (Budyko, 1977; Izrael, 2005; Crutzen, 2006; Wigley, 2006; Robock, 2008). In particular, based on an increase of diffuse sunlight after volcanic eruptions, Roderick et al. (2001) suggested that these eruptions (and, consequently, such proposed geoengineering scheme) would enhance terrestrial NPP. This suggestion was supported by the results of field experiments (Gu et al., 2003) but contradicts the results of tree–ring analyses (Krakauer and Randerson, 2003). Some suspicions about such enhancement was presented by Robock (2008) and were supported by model simulations by Angert et al. (2004). Notably, the terrestrial carbon cycle formulation in our model neglected difference between direct and diffuse solar radiation. As a result, terrestrial NPP_g decreased after volcanic eruptions in the model. However, the model reproduced negative excursions of the q_{CO_2} growth rate in these periods due to even stronger suppression of soil respiration. Moreover, it partly reproduced an f_{NPP} increase in northern forests after volcanic eruptions. Taking into account contradictions in empirical evidence on the response of NPP on volcanic eruptions, the simulations presented here lead to the conclusion that the described geoengineering scheme may diminish NPP rather than enhance it. This result does not invalidate an importance of diffuse light for terrestrial photosynthesis but contributes to the discussion on NPP response to volcanic eruptions and climate geoengineering via stratospheric sulfates.

Acknowledgements. The authors are indebted to L. L. Golubyatnikov and N. N. Zavalishin for discussions on the topic of the paper. The comments made by an anonymous reviewer greatly improved the text of the manuscript. Land-use scenarios were downloaded from the LUH project home site. This work was supported by the Programs of Russian Academy of Sciences, by the Russian Ministry for Education and Science, by the Russian Found for Basic Research, and by the Russian President Grant No. NSh–3301.2010.5.

APPENDIX

The Terrestrial Carbon Cycle Scheme Implemented in the IAP RAS CM

The basic variables of the terrestrial carbon cycle module are listed in Table A1.

Table A1. Basic variables of the terrestrial carbon cycle module.

Variable	Units	Description
$a_{\rm agro}$	non–dimensional	fraction of grid cell covered by natural vegetation
$a_{\rm fire}$	non–dimensional	fraction of grid cell burned annually due to natural fires
$a_{\rm nat}$	non–dimensional	fraction of grid cell covered by crops and pastures
$c_{\rm s}$	kg (C) m^{-2}	soil carbon stock per unit area
$c_{\rm v}$	kg (C) m^{-2}	vegetation carbon stock per unit area
d	kg (C) m^{-2} yr^{-1}	biomass disturbance per unit area
$e_{\rm fire}$	kg (C) m^{-2} yr^{-1}	CO_2 emissions due to natural fires per annum per unit area
$e_{\rm lu}$	kg (C) m^{-2} yr^{-1}	CO_2 emissions due to land use clearing per annum per unit area
$f_{\rm GPP}$	kg (C) m^{-2} yr^{-1}	vegetation gross primary production per annum per unit area
$f_{\rm l}$	kg (C) m^{-2} yr^{-1}	annual carbon uptake by terrestrail vegetation per unit area
$f_{\rm lf}$	kg (C) m^{-2} yr^{-1}	litter fall rate per annum per unit area
$f_{\rm NPP}$	kg (C) m^{-2} yr^{-1}	vegetation net primary production per annum per unit area
$q_{\rm CO_2}$	ppmv	CO_2 atmospheric content
$N_{\rm a}$	non–dimensional	the number of atmospheric time steps per year
$R_{\rm SW}$	W m^{-2}	shortwave radiation budget at the surface
$r_{\rm s}$	kg (C) m^{-2} yr^{-1}	heterotrophic respiration rate per unit area
$r_{\rm v}$	kg (C) m^{-2} yr^{-1}	autotrophic respiration rate per unit area
$T_{\rm a}$	K	surface air temperature
$T_{\rm veg}$	K	threshold temperature for grow season onset and withdrawal
w	non–dimensional	soil moisture content as a fraction of saturation
Lower indexes modifying the listed above variables		
j		indicates time instant within the year
Y		indicates fraction of grid cell covered either by natural vegetation (Y = nat) or by crops/pastures (Y = agro)
Z		indicates soil reservoir (fast, slow)

1. Living vegetation

The new, spatially distributed terrestrial carbon cycle module distinguishes six plant functional types (PFTs): tropical trees, temperate broadleaf trees, cool needleleaf trees, grasses, shrubs and crops. These PFTs are constructed based on the simplified Holdridge classes (Monserud and Leemans, 1992, as shown in Table A2). The model grid cell is divided in two parts covered by natural vegetation (one the first five above–mentioned PFTs; no more than one such PFT is allowed to reside in a given grid cell in the current version of the model) and crops, respectively. Fractional areas occupied by these parts hereafter denoted as $a_{\rm nat}$ and $a_{\rm agro}$ respectively. Equations for carbon mass per unit area in living vegetation $c_{\rm v,Y}$ (here and below Y depicts PFT) per unit area

$$\frac{\partial c_{\rm v,Y}}{\partial t} = f_{\rm GPP,Y} - r_{\rm v,Y} - f_{\rm lf,Y} - d_{\rm Y} \,, \qquad \text{(A1)}$$

where $f_{\rm GPP,Y}$, $r_{\rm v,Y}$, $f_{\rm lf,Y}$, and $d_{\rm Y}$ are gross primary production, autotrophic respiration, litterfall, and biomass disturbance per unit area.

Gross primary production (photosynthesis) was calculated according to

$$f_{\rm GPP,Y} = \frac{A_{\rm GPP}}{N_{\rm a}} g_1 \sum_{T_{\rm a,j} \geqslant T_{\rm veg}} g_2 g_3 R_{\rm SW,j} \,. \qquad \text{(A2)}$$

In Eq. (A2), the subindex j stands for the time instant within the year and $N_{\rm a}$ represents the number of time steps per year. Only time instants with surface air temperature $T_{\rm a,j} \geqslant T_{\rm veg} = 0°{\rm C}$ were included in the sum. Terrestrial plant fertilization by atmospheric CO_2 obeys the Michaelis–Menten law

$$g_1 = \frac{q_{\rm CO_2}}{q_{\rm CO_2} + q_{1/2}}$$

with half saturation constant $q_{1/2}$ which values 300 ppmv is a compromise between the respective values for C3 plants (Farquhar et al., 1980; Budyko and Izrae, 1991) and C4 plants (Collatz et al., 1992). The photosynthesis dependences on soil moisture fractional saturation w and surface air temperature read

$$g_2 = w_{\rm j} \,,$$

Table A2. Aggregated plant functional types implemented in the current IAP RAS CM version.

PFT implemented in the IAP RAS CM	Classes by Monserud and Leemans (1992)
tropical trees	tropical dry forest, tropical seasonal forest, tropical rain forest
temperate broadleaf trees	temperate forest, warm temperate forest
cool needleleaf trees	cool evergreen forest
grasses	tundra, steppe
shrubs	forest tundra, cold parklands, chapparal, tropical semi-arid
crops	crops

$$g_3 = \frac{Q_{10,\mathrm{GPP}}^{(T_{\mathrm{a,j}}-T_{\mathrm{opt,\ GPP}})/10}}{\{1+\exp[0.3(T_{\mathrm{a,\ j}}-T_{\mathrm{up,\ Y}})]\}\{1+\exp[0.3(T_{\mathrm{down,\ Y}}-T_{\mathrm{a,\ j}})]\}} .$$

In the latter equation $T_{\mathrm{up,Y}}$ and $T_{\mathrm{down,Y}}$ are PFT–dependent (Table A3), $Q_{10,\mathrm{GPP}} = 1.8$, and $T_{\mathrm{opt,GPP}} = 25°\mathrm{C}$. These values were based on Cox (2000). In Eq. (A2), it is additionally assumed that gross primary production depends linearly on available photosynthetic active radiation, and that photosynthetic active radiation is a fixed fraction of total shortwave radiation at the surface R_{SW}. The latter assumption is consistent with the atmospheric radiative transport module of the IAP RAS CM which does not distinguish between different solar spectral bands. This assumption is common for most climate models of intermediate complexity, e.g., the GENIE Earth system model (Lenton et al., 2006), the UVic ESCM (Weaver et al., 2001), and the McGill paleoclimate model (Wang et al., 2004). In addition, $f_{\mathrm{GPP,Y}}$ dependence on $c_{\mathrm{v,Y}}$, potentially important for natural vegetation with very small carbon stock (Svirezhev and von Bloh, 1997; Adams et al., 2004; Tarko, 2005) was neglected. Value of A_{GPP} is set to $3.58{\times}10^{-2}$ Pg (C) m^2 W^{-1} yr^{-1}.

Autotrophic respiration rate is computed based on the Arrhenius equation

$$r_{\mathrm{v,Y}} = \left[\frac{A_{\mathrm{v}}}{N_{\mathrm{a}}}\sum_{T_{\mathrm{a,j}}\geqslant T_{\mathrm{veg}}}\exp\left(-E_{\mathrm{v}}/RT_{\mathrm{a,j}}\right)\right] c_{\mathrm{v,Y}} , \quad \text{(A3)}$$

where $E_{\mathrm{v}} = 5.5\times10^4$ J mol^{-1} is activation energy (Williamson et al., 2006), R is universal gas constant, and $A_{\mathrm{v}} = 6.1\times10^8$ yr^{-1}.

For every PFT, fraction of leaves in total biomass $\alpha_{\mathrm{leaf,Y}}$ and turnaround times for leaves and wood ($\tau_{\mathrm{leaf,Y}}$ and $\tau_{\mathrm{wood,Y}}$, correspondingly) were prescribed (Table A3). As a result, leaf and wood masses per unit area are

$$\begin{aligned} c_{\mathrm{v,Y,leaf}} &= \alpha_{leaf} c_{\mathrm{v,Y}} \\ c_{\mathrm{v,Y,wood}} &= (1-\alpha_{\mathrm{leaf}})\, c_{\mathrm{v,Y}} . \end{aligned} \quad \text{(A4)}$$

Equations for leaf and wood litter fall rate in the model read

$$\begin{aligned} f_{\mathrm{lf,Y,leaf}} &= c_{\mathrm{v,Y,leaf}}/\tau_{\mathrm{leaf,Y}} , \\ f_{\mathrm{lf,Y,wood}} &= c_{\mathrm{v,Y,wood}}/\tau_{\mathrm{wood,Y}} . \end{aligned} \quad \text{(A5)}$$

Total litterfall rate is

$$f_{\mathrm{lf,Y}} = f_{\mathrm{lf,Y,leaf}} + f_{\mathrm{lf,Y,wood}} . \quad \text{(A6)}$$

2. Biomass disturbance

Biomass disturbance is a sum of contributions of natural fires and land–use clearing:

$$d_{\mathrm{Y}} = d_{\mathrm{fire,Y}} + d_{\mathrm{lu,Y}}, \quad \text{(A7)}$$

Biomass disturbance due to natural fires were parameterized according to Thonicke et al. (2001). Fire season length as a fraction of the Julian year in a given grid cell is

$$p_{\mathrm{fire}} = \frac{1}{N_{\mathrm{a}}}\sum_{T_{\mathrm{a,j}}>T_{\mathrm{veg}}}\exp[-\pi\,(w_{\mathrm{j}}/w_{\mathrm{e}})^2] .$$

Here $w_{\mathrm{e}} = 0.7$ stands for moisture of extinction. Fuel stock per unit area is

$$c_{\mathrm{fuel}} = \left(c_{\mathrm{v,Y,leaf}} + m_{\mathrm{fire,wood}} c_{\mathrm{v,Y,wood}}\right),$$

where $m_{\mathrm{fire,wood}} = 0.1$ is fraction of wood carbon stock burned annually. If $c_{\mathrm{fuel}} \geqslant c_{\mathrm{fuel},0} = 0.15$ kg (C) m^{-2} then fraction of grid cell area burnt annually is

$$a_{\mathrm{fire}} = (s+1)\exp\left(\frac{s}{0.45s^3+2.83s^2+2.96s+1.04}\right),$$

with $s = p_{\mathrm{fire}} - 1$. Otherwise, a_{fire} was set to zero. Annual biomass loss due to natural fires is considered to be equal to the respective CO_2 emissions in the atmosphere $e_{\mathrm{fire,Y}}$:

$$e_{\mathrm{fire,Y}} = d_{\mathrm{fire,Y}} = k_{\mathrm{res,Y}} c_{\mathrm{fuel}} a_{\mathrm{fire}} , \quad \text{(A8)}$$

with PFT–dependent resistance $k_{\mathrm{res,Y}}$ (Table A3). In turn, E_{fire} in Eq. (1) was calculated from $e_{\mathrm{fire,Y}}$ by multiplying either by a_{nat} or by a_{agro}, then multiplying by grid cell area and summing globally.

Table A3. PFT–dependent values for the governing parameters of the IAP RAS CM terrestrial carbon cycle routine. Index used in the body of the text to indicate PFT type is dropped in this Table for simplicity.

PFT	$T_{\rm up}$ (°C)	$T_{\rm down}$ (°C)	$\alpha_{\rm leaf}$	$\tau_{\rm leaf}$ (yr)	$\tau_{\rm wood}$ (yr)	$k_{\rm res}$
tropical trees	36	0	0.07	1	167	0.5
temperate broadleaf trees	31	0	0.07	2	167	0.12
cool needleleaf trees	31	−5	0.07	1	143	0.5
grasses	34	0	0.9	1	5	1.0
shrubs	34	0	0.3	1	10	0.12
crops	34	0	0.9	1	20	0.1

Table A4. Values for the governing parameters of the soil compartment of the IAP RAS CM terrestrial carbon cycle routine. Lower indexes used in the body of the text to indicate vegetation and soil pool type were omitted in this table for simplicity.

Vegetation type	Soil pool	$Q_{10,\rm s}$	$A_{\rm s}$ (yr^{-1})
natural	fast	2.2	0.15
	slow	1.5	0.04
agricultural	fast	2.2	0.20
	slow	1.5	0.05

Disturbance due to land–use clearing from year k to year k + 1 is

$$d_{\rm lu,nat} = c_{\rm v,nat} \times \max\left[\left(a_{\rm nat}^{(k+1)} - a_{\rm nat}^{(k)}\right),\ 0\right]. \quad \text{(A9)}$$

For the fraction of cell covered by agriculture, $d_{\rm lu,agro} = 0$. It was assumed that corresponding amount of carbon was released to the atmosphere in the form of CO_2 during 1 year (Brovkin et al., 2004). Therefore, annual CO_2 emissions due to land–use clearing are

$$e_{\rm lu} = d_{\rm nat,lu}. \quad \text{(A10)}$$

The procedure to calculate $E_{\rm lu}$ in Eq. (1) from $e_{\rm lu}$ is similar to the respective procedure for computation of $E_{\rm fire}$. Possible delay in land–use clearing emissions due to incomplete burning of cut biomass Houghton et al., (e.g., 1983) was neglected. One notes that emissions defined as in Eq. (A10) correspond to the so–called direct emissions. Indirect land–use emissions related to soil cultivation and vegetation regrowth after crop abandonment (Houghton et al., 1983) were described by the corresponding parameterizations in the present carbon cycle scheme.

3. Soil carbon dynamics

Soil carbon was divided in two pools, with fast and slow turnaround times, respectively. Hereafter, variables related to these pools are denoted by lower indexes Z = fast, slow. Budget equation for carbon in these pools are (Houghton et al., 1983)

$$\frac{\partial c_{\rm s,Y,Z}}{\partial t} = f_{\rm lf,Y,Z} - r_{\rm s,Y,Z}. \quad \text{(A11)}$$

For simplicity, it was assumed that $f_{\rm lf,Y,fast} = f_{\rm lf,Y,leaf}$ and $f_{\rm lf,Y,slow} = f_{\rm lf,Y,wood}$.

Heterotrophic respiration calculation was based on the TRIFFID model (Cox, 2000):

$$r_{\rm s,Y,Z} = \left[\frac{A_{\rm s,Y,Z}}{N_{\rm a}} \sum_{T_{\rm a,j} > T_{\rm veg}} g_4 g_5\right] c_{\rm s,Y,Z}, \quad \text{(A12)}$$

with

$$g_4 = \begin{cases} 0.2, & w < w_{\rm wilt} \\ 0.2 + 0.8\,(w - w_{\rm wilt})\,/\,(w_{\rm opt} - w_{\rm wilt}), & w_{\rm wilt} \geqslant w \geqslant w_{\rm opt} \\ 1 - 0.8\,(w - w_{\rm opt}), & w > w_{\rm opt} \end{cases},$$

$$g_5 = Q_{10,\rm s,Z}^{(T - T_{\rm opt,s})/10},$$

where wilting moisture $w_{\rm wilt} = 0.2$, optimal values for moisture and temperature are $w_{\rm opt} = (1/2)\,(w_{\rm wilt} + 1)$

and $T_{\mathrm{opt,s}} = 25°\mathrm{C}$, respectively. Values for $Q_{10,\mathrm{s,Z}}$ and $A_{\mathrm{s,Y,Z}}$ are listed in Table A4. Values for $A_{\mathrm{s,Y,Z}}$ in the case of Y = agro are larger in comparison to the respective values for Y = nat by 30% in order to represent impact of cultivation on soil respiration (Piao et al., 2009).

In the case of land–use clearing or crop abandonment from year k to year k + 1, soil carbon is recalculated to conserve the total amount of carbon in soil within a grid cell:

- clearing: $a_{\mathrm{agro}}^{(\mathrm{k}+1)} > a_{\mathrm{agro}}^{(\mathrm{k})}$:

$$c_{\mathrm{s,nat}}^{(\mathrm{k}+1)} = c_{\mathrm{s,nat}}^{(\mathrm{k})} ;$$

$$c_{\mathrm{s,agro}}^{(\mathrm{k}+1)} = \left[c_{\mathrm{s,nat}}^{(\mathrm{k})} \left(a_{\mathrm{agro}}^{(\mathrm{k}+1)} - a_{\mathrm{agro}}^{(\mathrm{k})} \right) + c_{\mathrm{s,\,agro}}^{(\mathrm{k})} a_{\mathrm{agro}}^{(\mathrm{k})} \right] / a_{\mathrm{agro}}^{(\mathrm{k}+1)} ;$$

- abandonment: $a_{\mathrm{agro}}^{(\mathrm{k}+1)} < a_{\mathrm{agro}}^{(\mathrm{k})}$:

$$c_{\mathrm{s,nat}}^{(\mathrm{k}+1)} = \left[c_{\mathrm{s,agro}}^{(\mathrm{k})} \left(a_{\mathrm{agro}}^{(\mathrm{k})} - a_{\mathrm{agro}}^{(\mathrm{k}+1)} \right) + c_{\mathrm{s,nat}}^{(\mathrm{k})} a_{\mathrm{nat}}^{(\mathrm{k})} \right] / a_{\mathrm{agro}}^{(\mathrm{k}+1)} ;$$

$$c_{\mathrm{s,agro}}^{(\mathrm{k}+1)} = c_{\mathrm{s,agro}}^{(\mathrm{k})} .$$

4. Net primary production and terrestrial carbon uptake

Terrestrial net primary production is

$$f_{\mathrm{NPP}} = \sum_{\mathrm{Y=nat,\ agro}} a_{\mathrm{Y}} \left(f_{\mathrm{GPP,Y}} - r_{\mathrm{v,Y}} \right).$$

The respective terrestrial carbon uptake is calculated as

$$f_{\mathrm{l}} = \textstyle\sum_{\mathrm{Y=nat,\ agro}} a_{\mathrm{Y}} \left(f_{\mathrm{NPP,Y}} - r_{\mathrm{s,Y}} - e_{\mathrm{fire,Y}} \right) .$$

REFERENCES

Adams, B., A. White, and T. M. Lenton, 2004: An analysis of some diverse approaches to modelling terrestrial net primary productivity. *Ecological Modelling*, **177**, 353–391.

Ammann, C. M., G. A. Meehl, W. M. Washington, and C. S. Zender, 2003: A monthly and latitudinally varying volcanic forcing dataset in simulations of 20th century climate. *Geophys. Res. Lett.*, **30**(12), 1657.

Angert, A., S. Biraud, C. Bonfils, and I. Fung, 2004: CO_2 seasonality indicates origins of post–Pinatubo sink. *Geophys. Res. Lett.*, **31**(11), L11103.

Arora, V. K., and H. D. Matthews, 2009: Characterizing uncertainty in modeling primary terrestrial ecosystem processes. *Global Biogeochemical Cycles*, **23**(2), GB2016.

Arzhanov, M. M., P. F. Demchenko, A. V. Eliseev, and I. I. Mokhov, 2008: Simulation of characteristics of thermal and hydrologic soil regimes in equilibrium numerical experiments with a climate model of intermediate complexity. *Izvestiya, Atmospheric and Oceanic Physics*, **44**(5), 279–287.

Bacastow, B., 1981: Numerical evaluation of the evasion factor. *Carbon Cycle Modelling, SCOPE–16*, B. Bolin, Ed., J. Wiley and Sons, N. Y., 95–101.

Brovkin, V., J. Bendtsen, M. Claussen, A. Ganopolski, C. Kubatzki, V. Petoukhov, and A. Andreev, 2002: Carbon cycle, vegetation, and climate dynamics in the Holocene: Experiments with the CLIMBER–2 model. *Global Biogeochemical Cycles*, **16**(4), 1139.

Brovkin, V., S. Sitch, W. von Bloh, M. Claussen, E. Bauer, and W. Cramer, 2004: Role of land cover changes for atmospheric CO_2 increase and climate change during the last 150 years. *Global Change Biology*, **10**, 1253–1266.

Budyko, M. I., 1977: *Climate Changes*. American Geophysical Union, Washington, D. C., 261pp.

Budyko, M. I., and Y. A. Izrae, Eds., 1991: *Anthropogenic Climate Change*. Arizona Univ. Press, Tucson, 485pp.

Collatz, G. J., M. Ribas-Carbo, and J. A. Berry, 1992: Coupled photosynthesis-stomatal conductance model for leaves of C_4 plants. *Australian Journal of Plant Physiology* , **19**(5), 519–538.

Cox, P. M., 2000: Description of the TRIFFID dynamic global vegetation model. Technical Report Hadley Centre technical note 24, Hadley Centre, Met. Office, Bracknell.

Cox, P. M., R. A. Betts, C. D Jones, S. A. Spall, and I. J. Totterdell, 2000: Acceleration of global warming due to carbon-cycle feedbacks in a coupled climate model. *Nature*, **408**(6809), 184–187.

Cramer, W., and Coauthors, 2001: Global response of terrestrial ecosystem structure and function to CO_2 and climate change: Results from six dynamic global

vegetation models. *Global Change Biology*, **7**(4), 357–373.

Cramer, W., D. W. Kicklighter, A. Bondeau, B. Moore, G. Churkina, B. Nemry, A. Ruimy, A. L. Schloss, and Participants of the Potsdam NPP model intercomparison, 1999: Comparing global models of terrestrial net primary productivity (NPP): Overview and key results. *Global Change Biology*, **5**(Suppl.1), 1–15.

Crutzen, P. J., 2006: Albedo enhancement by stratospheric sulfur injections: A contribution to resolve a policy dilemma? *Climatic Change*, **77**(3–4), 211–219.

DeFries, R. S., C. B. Field, I. Fung, G. J. Collatz, and L. Bounoua, 1999: Combining satellite data and biogeochemical models to estimate global effects of human–induced land cover change on carbon emissions and primary productivity. *Global Biogeochemical Cycles*, **13**(3), 803–815.

Eliseev, A. V., 2008: Estimation of the uncertainty of future changes in atmospheric carbon dioxide concentration and its radiative forcing. *Izvestiya, Atmospheric and Oceanic Physics*, **44**(3), 279–287.

Eliseev, A. V., 2011: An assessment of climate and carbon cycle changes in the 21st century taking into account uncertainty in values of governing parameters for terrestrial biota. *Izvestiya, Atmospheric and Oceanic Physics*, **47**(2), 131–153.

Eliseev, A. V., M. M. Arzhanov, P. F. Demchenko, and I. I. Mokhov, 2009: Changes in climatic characteristics of Northern Hemisphere extratropical land in the 21st century: Assessments with the IAP RAS climate model. *Izvestiya, Atmospheric and Oceanic Physics*, **45**(3), 271–283.

Eliseev, A. V., and I. I. Mokhov, 2007: Carbon cycle–climate feedback sensitivity to parameter changes of a zero–dimensional terrestrial carbon cycle scheme in a climate model of intermediate complexity. *Theor. Appl. Climatol.*, **89**(1–2), 9–24.

Eliseev, A. V., and I. I. Mokhov, 2008: Eventual saturation of the climate–carbon cycle feedback studied with a conceptual model. *Ecological Modelling*, **213**(1), 127–132.

Eliseev, A. V., and I. I. Mokhov, 2011: Impact of radiative effect of albedo changes due to land use on results of simulations with the climate model. *Izvestiya, Atmospheric and Oceanic Physics*, **47**(1), 15–39.

Eliseev, A. V., I. I. Mokhov, M. M. Arzhanov, P. F. Demchenko, and S. N. Denisov, 2008: Interaction of the methane cycle and processes in wetland ecosystems in a climate model of intermediate complexity. *Izvestiya, Atmospheric and Oceanic Physics*, **44**(2), 139–152.

Eliseev, A. V., I. I. Mokhov, and A. A. Karpenko, 2007a: Climate and carbon cycle variations in the 20th and 21st centuries in a model ofintermediate complexity. *Izvestiya, Atmospheric and Oceanic Physics*, **43**(1), 1–14.

Eliseev, A. V., I. I. Mokhov, and A. A. Karpenko, 2007b: Influence of direct sulfate–aerosol radiative forcing on the results of numerical experiments with a climate model of intermediate complexity. *Izvestiya, Atmospheric and Oceanic Physics*, **42**(5), 544–554.

Farquhar, G. D., S. von Caemmerer, and J. A. Berry, 1980: A biochemical model of photosynthetic CO_2 assimilation in leaves of C_3 species. *Planta*, **149**(1), 78–90.

Friedlingstein, P., L. Bopp, P. Ciais, J.-L. Dufresne, L. Fairhead, H. Le Treut, P. Monfray, and J. Orr., 2001: Positive feedback between future climate change and the carbon cycle. *Geophys. Res. Lett.*, **28**(8), 1543–1546.

Friedlingstein, P., and Coauthors, 2006: Climate–carbon cycle feedback analysis: Results from the C^4MIP model intercomparison. *J. Climate*, **19**(22), 3337–3353.

Gedney, N., P. M. Cox, and C. Huntingford, 2004: Climate feedback from wetland methane emissions. *Geophys. Res. Lett.*, **31**(20), L20503.

Gerber, S., L. O. Hedin, M. Oppenheimer, S. W. Pacala, and E. Shevliakova, 2010: Nitrogen cycling and feedbacks in a global dynamic land model. *Global Biogeochemical Cycles*, **24**(1), GB1001.

Ginzburg, A. S., and N. N. Zavalishin, 2008: Dynamics of a closed low–parameter compartment model of the global carbon cycle. *Izvestiya, Atmospheric and Oceanic Physics*, **44**(6), 684–700.

Goldewijk, K. K., 2001: Estimating global land use change over the past 300 years: the HYDE database. *Global Biogeochemical Cycles*, **15**(2), 417–434.

Golubyatnikov, L. L., and E. A. Denisenko, 2001: Modeling the values of net primary production for the zonal vegetation in European Russia. *Biology Bulletin*, **28**(3), 293–300, doi: 10.1023/A:1016648722322.

Gu, L., D. D. Baldocchi, S. C. Wofsy, J. W. Munger, J. J. Michalsky, S. P. Urbanski, and T. A. Boden, 2003: Response of a deciduous forest to the Mount Pinatubo eruption: Enhanced photosynthesis. *Science*, **299**(5615), 2035–2038.

Hall, F. G., G. Collatz, S. Los, E. Brown de Colstoun, and D. Landis, Eds., 2005: ISLSCP Initiative II. NASA, Greenbelt Md., digital media.

Handorf, D., V. K. Petoukhov, K. Dethloff, A. V. Eliseev, A. Weisheimer, and I. I. Mokhov, 1999: Decadal climate variability in a coupled atmosphere-ocean climate model of moderate complexity. *J. Geophys. Res.*, **104**(D22), 27253–27275.

Horowitz, L. W., 2006: Past, present, and future concentrations of tropospheric ozone and aerosols: Methodology, ozone evaluation, and sensitivity to aerosol wet deposition. *J. Geophys. Res.*, **111**(D22), D22211.

Houghton, J. T., Y. Ding, D. J. Griggs, M. Noguer, P. J. van der Linden, X. Dai, K. Maskell, and C. A. Johnson, Eds., 2001: *Climate Change 2001: The Scientific Basis. Contribution of Working Group I to the Third Assessment Report of the Intergovernmental Panel on Climate Change*, Cambridge University Press, Cambridge/New York, 892pp.

Houghton, R. A., J. E. Hobbie, J. M. Melillo, B. Moore, B. J. Peterson, G. R. Shaver, and G. M. Woodwell, 1983: Changes in the carbon content of terrestrial biota and soils between 1860 and 1980: A net release of CO_2 to the atmosphere. *Ecological Monographs*, **53**(3), 235–262.

Houlton, B. Z., Y.-P. Wang, P. M. Vitousek, and C. B. Field, 2008: A unifying framework for dinitrogen fixation in the terrestrial biosphere. *Nature*, **454**(7202), 327–330.

Hurtt, G. C., and Coauthors, 2009: Harmonization of global land–use scenarios for the period 1500–2100 for IPCC–AR5. *Integrated Land Ecosystem-Atmosphere Processes Study* (*iLEAPS*) *Newsletter*, (7), 6–8.

Izrael, Yu. A., 2005: An efficient way to regulate global climate is the main goal of the climate problem solution. *Russian Meteorology and Hydrology*, **30**(10), 1–4.

Jain, A., X. Yang, H. Kheshgi, A. D. McGuire, W. Post, and D. Kicklighter, 2009: Nitrogen attenuation of terrestrial carbon cycle response to global environmental factors. *Global Biogeochemical Cycles*, **23**(4), GB4028.

Jobbágy, E. G., and R. B. Jackson, 2000: The vertical distribution of soil organic carbon and its relation to climate and vegetation. *Ecological Applications*, **10**(2), 423–486.

Jones, C. D., and P. M. Cox, 2001: Constraints on the temperature sensitivity of global soil respiration from the observed interannual variability in atmospheric CO_2. *Atmos. Sci. Lett.*, **2**(1–4), 166–172.

Jones, C. D., P. M. Cox, and C. Huntingford, 2006: Climate–carbon cycle feedbacks under stabilisation: Uncertainty and observational constraints. *Tellus*, **58B**(5), 603–613.

Keeling, C. D., J. F. S. Chine, and T. P. Whorf, 1996: Increased activity of northern vegetation inferred from atmospheric CO_2 measurements. *Nature*, **382**, 146–149.

Krakauer, N. Y., and J. T. Randerson, 2003: Do volcanic eruptions enhance or diminish net primary production? Evidence from tree rings. *Global Biogeochemical Cycles*, **17**(4), 1118.

Lenton, T. M., and Coauthors, 2006: Millennial timescale carbon cycle and climate change in an efficient Earth system model. *Climate Dyn.*, **26**(7–8), 687–711.

Lewis, S. L., and Coauthous, 2009: Increasing carbon storage in intact African tropical forests. *Nature*, **457**(7232), 1003–1006.

Luyssaert, S., and Coauthors, 2007: CO_2 balance of boreal, temperate, and tropical forests derived from a global database. *Global Change Biology*, **13**(12), 2509–2537.

MacFarling Meure, C., D. Etheridge, C. Trudinger, P. Steele, R. Langenfelds, T. van Ommen, A. Smith, and J. Elkins, 2006: Law Dome CO_2, CH_4 and N_2O ice core records extended to 2000 years BP. *Geophys. Res. Lett.*, **33**(14), L14810.

Marland, G., T. A. Boden, and R. J. Andres, 2005: Global, regional, and national CO_2 emissions. In *Trends: A Compendium of Data on Global Change*. Carbon Dioxide Information Analysis Center, Oak Ridge National Laboratory, U. S. Department of Energy, Oak Ridge, Tenn.

Matthews, H. D., A. J. Weaver, and K. J. Meissner, 2005: Terrestrial carbon cycle dynamics under recent and future climate change. *J. Climate*, **18**(10), 1609–1628.

Matthews, H. D., A. J. Weaver, K. J. Meissner, N. P. Gillett, and M. Eby, 2004: Natural and anthropogenic climate change: Incorporating historical land cover change, vegetation dynamics and the global carbon cycle. *Climate Dyn.*, **22**(5), 461–479.

Millero, F. J., 1995: Thermodynamics of carbon dioxide system in the ocean. *Geochimica et Cosmochimica Acta*, **59**(4), 661–677.

Mokhov, I. I., and A. V Eliseev, 2008: Explaining the eventual transient saturation of climate–carbon cycle feedback. *Carbon Balance Management*, **3**(4), doi: 10.1186/1750-0680-3-4.

Mokhov, I. I., and Coauthors, 2005: Climate changes and their assessment based on the IAP RAS global model simulations. *Doklady Earth Sciences*, **402**(4), 591–595.

Mokhov, I. I., A. V. Eliseev, and A. A. Karpenko, 2006: Sensitivity of the IAP RAS Global Climatic Model with an interactive carbon cycle to anthropogenic influence. *Doklady Earth Sciences*, **407**(3), 424–428.

Mokhov, I. I., A. V. Eliseev, and A. A. Karpenko, 2008: Decadal–to–centennial scale climate–carbon cycle interactions from global climate models simulations forced by anthropogenic emissions. *Climate Change Reseacrh Trends*, L. N. Peretz, Ed., Nova Sci. Publ., Hauppauge, NY, 217–241.

Monserud, R. A., and R. Leemans, 1992: Comparing global vegetation maps with the Kappa statistic. *Ecological Modelling*, **62**(4), 275–293.

Nemani, R. R., C. D. Keeling, H. Hashimoto, W. M. Jolly, S. C. Piper, C. J. Tucker, R. B. Myneni, and S. W. Running, 2003: Climate–driven increases in global terrestrial net primary production from 1982 to 1999. *Science*, **300**(5625), 1560–1563.

Olofsson, J., and T. Hickler, 2008: Effects of human land–use on the global carbon cycle during the last 6,000 years. *Veg. Hist. Archeobot.*, **17**(5), 605–615.

Olson, J. S., J. A. Watts, and L. A. Allison, 1985: Major world ecosystem complexes ranked by carbon in live vegetation. Technical Report NDP-017, Carbon Dioxide Information Center, Oak Ridge National Laboratory, Oak Ridge, Tennessee.

Petoukhov, V., and Coauthour, 2005: EMIC intercomparison project (EMIP–CO_2): Comparative analysis of EMIC simulations of current climate and equilibrium and transient reponses to atmospheric CO_2 doubling. *Climate Dyn.*, **25**(4), 363–385.

Petoukhov, V. K., I. I. Mokhov, A. V. Eliseev, and V. A. Semenov, 1998: *The IAP RAS Global Climate Model.*

Dialogue–MSU, Moscow.

Piao, S., P. Ciais, P. Friedlingstein, N. de Noblet-Ducoudré, P. Cadule, N. Viovy, and T. Tao Wang, 2009: Spatiotemporal patterns of terrestrial carbon cycle during the 20th century. *Global Biogeochemical Cycles*, **23**(4), GB4026.

Pongratz, J., C. H. Reick, T. Raddatz, and M. Claussen, 2009: Effects of anthropogenic land cover change on the carbon cycle of the last millennium. *Global Biogeochemical Cycles*, **23**(4), GB4001.

Robertson, A., and Coauthors, 2001: Hypothesized climate forcing time series for the last 500 years. *J. Geophys. Res.*, **106**(D14), 14783–14804.

Robock, A., 2008: 20 reasons why geoengineering may be a bad idea. *Bull. Atmos. Sci.*, **64**(2), 14–18.

Roderick, M. L., G. D. Farquhar, S. L. Berry, and I. R. Noble, 2001: On the direct effect of clouds and atmospheric particles on the productivity and structure of vegetation. *Oecologia*, **129**(1), 21–30.

Sabine, C. L., and Coauthors, 2004: The oceanic sink for anthropogenic CO_2. *Science*, **305**, 367–371.

Schultz, M. G., and Coauthors, 2008: Global wildland fire emissions from 1960 to 2000. *Global Biogeochemical Cycles*, **22**(2), GB2002.

Sokolov, A. P., D. W. Kicklighter, J. M. Melillo, B. S. Felzer, C. A. Schlosser, and T. W. Cronin, 2008: Consequences of considering carbon–nitrogen interactions on the feedbacks between climate and the terrestrial carbon cycle. *J. Climate*, **21**(15), 3776–3796.

Solomon, S., D. Qin, M. Manning, M. Marquis, K. Averyt, M. M. B. Tignor, H. LeRoy Miller, and Z. Chen, Eds., 2007: *Climate Change 2007: The Physical Science Basis*. Cambridge University Press, Cambridge/New York.

Strassmann, K. M., F. Joos, and G. Fischer, 2008: Simulating effects of land use changes on carbon fluxes: Past contributions to atmospheric CO_2 increases and future commitments due to losses of terrestrial sink capacity. *Tellus*, **60B**(4), 583–603.

Svirezhev, Yu. M., V. Brovkin, W. von Bloh, H. J. Schellnhuber, and G. Petschel-Held, 1999: Optimisation of reduction of global CO_2 emission based on a simple model of the carbon cycle. *Environmental Modeling & Assessment*, **4**(1), 23–33.

Svirezhev, Yu. M., and W. von Bloh, 1997: Climate, vegetation, and global carbon cycle: The simplest zero–dimensional model. *Ecological Modelling*, **101**, 79–95.

Svirezhev, Yu. M., and W. von Bloh, 1998: A zero–dimensional climate–vegetation model containing global carbon and hydrological cycle. *Ecological Modelling*, **106**, 119–127.

Tarko, A. M., 2005: *Anthropogenic Changes of Global Biospheric Processes. Mathematical Modelling*. Fizmatlit, Moscow, 232pp. (in Russian)

Thonicke, K., S. Venevsky, S. Sitch, and W. Cramer, 2001: The role of fire disturbance for global vegetation dynamics: coupling fire into a Dynamic Global Vegetaion Model. *Global Ecology and Biogeography*, **10**(6), 661–677.

Thornton, P. E., J.-F. Lamarque, N. A. Rosenbloom, and N. M. Mahowald, 2007: Influence of carbon-nitrogen cycle coupling on land model response to CO_2 fertilization and climate variability. *Global Biogeochemical Cycles*, **21**(4), GB4018.

Volodin, E. M., 2007: Atmosphere–ocean general circulation model with the carbon cycle. *Izvestiya, Atmospheric and Oceanic Physics*, **43**(3), 266–280.

Volodin, E. M., 2008: Methane cycle in the INM RAS climate model. *Izvestiya, Atmospheric and Oceanic Physics*, **44**(2), 153–159.

Walker, S. J., R. F. Weiss, and P. K. Salameh, 2000: Reconstructed histories of the annual mean atmospheric mole fractions for the halocarbons CFC–11, CFC–12, CFC–113 and carbon tetrachloride. *J. Geophys. Res.*, **105**(C6), 14285–14296.

Wang, Y.-M., J. Lean, and N. R. Sheeley, 2005: Modeling the Sun's magnetic field and irradiance since. *The Astrophysical Journal*, **625**(1), 522–538.

Wang, Z., R.-M. Hu, L. A. Mysak, J.-P. Blanchet, and J. Feng, 2004: A parameterization of solar energy disposition in the climate system. *Atmos.–Ocean*, **42**(2), 113–125.

Weaver, A. J., and Coauthors, 2001: The UVic Earth system climate model: Model description, climatology, and applications to past, present and future climates. *Atmos.–Ocean*, **39**(4), 361–428.

Wigley, T. M. L., 2006: A combined mitigation/ geoengineering approach to climate stabilization. *Science*, **314**(5798), 452–454.

Williamson, M. S., T. M. Lenton, J. G. Shepherd, and N. R. Edwards, 2006: An efficient numerical terrestrial scheme (ENTS) for Earth system modelling. *Ecological Modelling*, **198**, 362–374.

Zaehle, S., P. Friedlingstein, and A. D. Friend, 2010a: Terrestrial nitrogen feedbacks may accelerate future climate change. *Geophys. Res. Lett.*, **37**(1), L01401.

Zaehle, S., A. D. Friend, P. Friedlingstein, F. Dentener, P. Peylin, and M. Schulz, 2010b: Carbon and nitrogen cycle dynamics in the O–CN land surface model: 2. role of the nitrogen cycle in the historical terrestrial carbon balance. *Global Biogeochemical Cycles*, **24**(1), GB1006.

Zhao, M., S. W. Running, and R. R. Nemani, 2006: Sensitivity of Moderate Resolution Imaging Spectroradiometer (MODIS) terrestrial primary production to the accuracy of meteorological reanalyses. *J. Geophys. Res.*, **111**(G1), G01002.

Zickfeld, K., M. Eby, and A. J. Weaver, 2008: Carbon–cycle feedbacks of changes in the Atlantic meridional overturning circulation under future atmospheric CO_2. *Global Biogeochemical Cycles*, **22**(3), GB3024.